Journal of Civil Engineering and Management
ISSN 1392-3730/eISSN 1822-3605
2022 Volume 28 Issue 5: 397–407
https://doi.org/10.3846/jcem.2022.16825

STUDY ON SEISMIC RESPONSE OF A NEW STAGGERED STORY ISOLATED STRUCTURE CONSIDERING SSI EFFECT

Dewen LIU[1], Liping LI[2*], Yafei ZHANG[3#], Lihao CHEN[1], Feng WAN[1], Fan YANG[1]

[1]*College of Civil Engineering, Southwest Forestry University, Kunming, China*
[2]*Department of Civil Engineering, Faculty of Engineering, Lishui University, Lishui, China*
[3]*School of Civil Engineering, Tianjin University, Tianjin, China*

Received 10 August 2021; accepted 23 February 2022

Abstract. The new staggered story isolated structure is a new type of seismic isolated structure developed from base isolated structure and inter-story isolated structure. In order to explore the seismic response of the new staggered story isolated structure considering the soil-structure interaction (SSI), the model of a new staggered story isolated structure considering SSI effect is established to analyze the nonlinear dynamic time-history response under rare earthquakes, and the comparison between hard soil and soft soil was carried out. Results show that the stiffness of the new staggered story isolated structure reduced, the modal period extended and the seismic response reduced by considering the SSI effect, the softer the site soil, the more obvious those changes are. Meanwhile, the shear force and the damage of the core tube decreases, while the shear force and the damage of the frame increases, the shear force transfers from the core tube to the frame. Additionally, the energy absorption of the seismic isolated bearings at the frame reduced, the energy absorption of the seismic isolated bearings at the core tube increased, the softer the site soil, the more obvious the trend is.

Keywords: SSI effect, new staggered story isolated structure, vibration absorption, damage.

Introduction

The new staggered story isolated (NSSI) structure is a new type of seismic isolated structure developed from the base isolated structure and the inter-story isolated structure. The characteristic of the base isolated structure is the isolated layer lies at the bottom of the structure, as shown in Figure 1a. The characteristic of the inter-story isolated structure is the isolated layer lies in the middle of the structure, as shown in Figure 1b. The seismic isolated layer of the new staggered story isolated structure is divided into two parts, the seismic isolated layer of the core tube part is located at the bottom of the core tube, forming a similar base isolated mode, the seismic isolated layer of the frame part is located in the middle of the structure, forming a similar inter-story isolated mode, as shown in Figure 1c. The advantage of the new staggered story isolated structure is the integrity of the core tube is ensured compared with the inter-story isolated structure. The Huafa Project in Baotou, Inner Mongolia, China is a representative building of the new staggered story isolated structure, as shown in Figure 2 (Zhang, 2019), and the seismic isolated layer is shown in Figure 3. The structure has a large chassis with two towers, as shown in Figure 3,

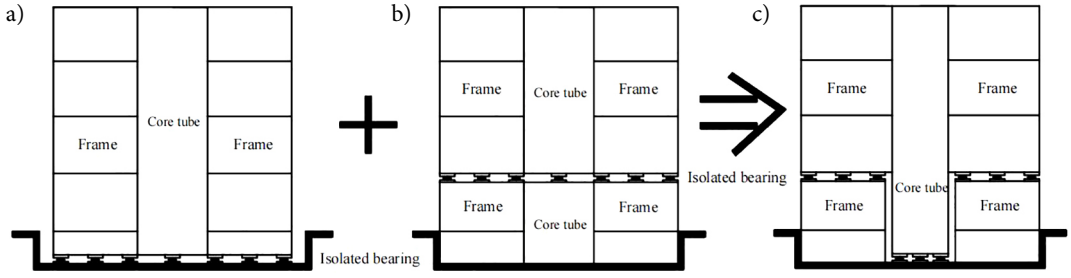

Figure 1. Structure diagram: a – base isolated structure; b – inter-story isolated structure; c – new staggered story isolated structure

*Corresponding author. E-mail: *llp@lsu.edu.cn*
#Corresponding author. E-mail: *zhangyf95@tju.edu.cn*

if it is designed into base isolated structure, it will bring vertical irregular problems.

The base isolated structures are widely used and studied (Kelly, 2012; Castaldo & Tubaldi, 2018; Zhou et al., 2018; Shan et al., 2020; Shang & Hu, 2020). The development of inter-story isolated structures is relatively later than the base isolated structures, and the research on inter-story isolated structures is increasing year by year (Zhang et al., 2009; Zhou et al., 2016; Chang & Zhu, 2011; Loh et al., 2013). There are few studies about the new staggered story isolated structures, Liufu et al. (2020) and Qi et al. (2020) conducted preliminary studies on a new staggered story isolated structure, which showed that the structure had good performance under earthquakes. Korean scholars Kubin et al. (2012) studied a new staggered story isolated structure which is a hospital, showed that it had a good vibration absorption effect.

The above studies are based on rigid foundation assumption and the influence of soil-structure interaction (SSI effect) were not be considered. Karabork et al. (2014), Zhuang et al. (2014), Liu et al. (2013) and Li et al. (2012) studied the effect of the base isolated structure considering the SSI effect, Zhang et al. (2014) and Su et al. (2015) studied the inter-story isolated structure considering the SSI effect. Results showed that the seismic response were different by considering SSI effect.

The seismic response of the new staggered story isolated structure considering SSI effect has not yet been studied. This paper establishes a finite element model of a new staggered story isolated structure considering SSI effect to perform nonlinear dynamic time-history analysis under rare earthquakes, and provides a certain reference for the application of the new staggered story isolated structure.

Figure 2. A new staggered story isolated structure in Baotou, China

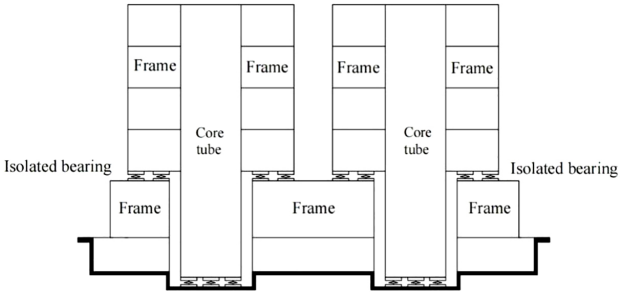

Figure 3. Structure diagram of the new staggered story isolated structure in Baotou, China

1. Finite element model of a new staggered story isolated structure

1.1. Project summary

The finite element model of a 18-story new staggered story isolated structure considering SSI effect is established by ETABS, as shown in Figure 4a. For comparative analysis, the finite element model of the new staggered story isolated structure without the SSI effect is also established, as shown in Figure 4b. As shown in Figure 5, according to China's seismic code (GB 50011-2010) (Ministry of Housing and Urban-rural Construction of the People's Republic of China and the General Administration of Quality Supervision, Inspection and Quarantine of the People's Republic of China, 2016), the building lies at a high-intensity earthquake area, the site category is Class II or III, and the seismic fortification intensity is 8 degrees. The basic seismic acceleration is 0.20 g. The building adopts a frame-core tube structure with a plane size of 30 m × 15 m, total

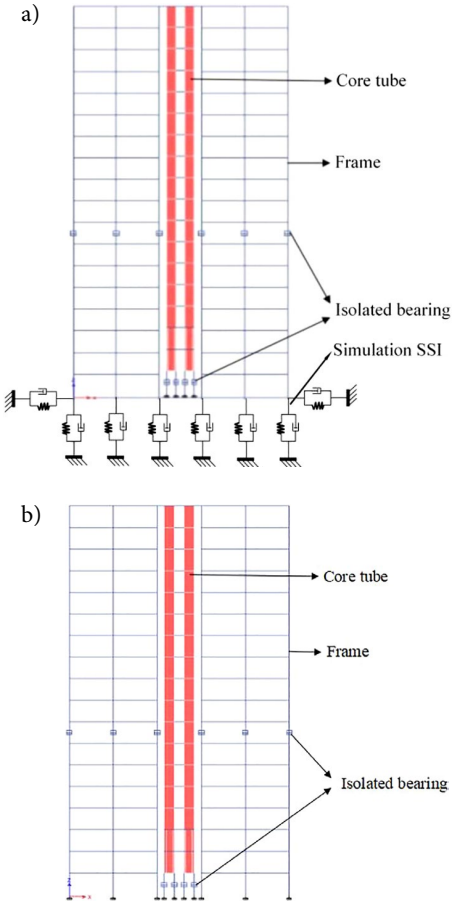

Figure 4. Model diagram of the new staggered story isolated structure: a – considering SSI effect; b – not considering SSI effects

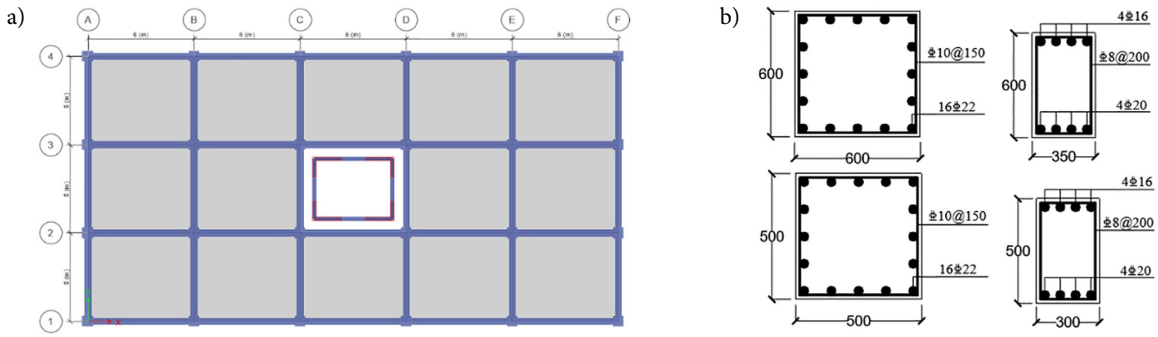

Figure 5. New staggered story isolated structure diagram: a – structural plane diagram; b – structural reinforcement drawing

height of 65.2 m, the first floor height of 4 m, and the standard story height of 3.6 m. The structure has a shallow foundation and the seismic isolated layer is located at the top of 7th floor of the frame and the bottom of the core tube. The floors below 8th story are shopping mall and the floors above 8th story is apartment. The concrete strength grade of frame column and core tube is defined as C40 and the frame beam is defined as C30, the floor plate thickness is 100 mm. The thickness of the protective layer of the beam and column is 50 mm. All types of rebars are HRB400. The information of frame beams, columns and stirrup are shown in Table 1, the information of core tube shear wall is shown in Table 2.

1.2. Nonlinear parameters of the new staggered story isolated structure

The seismic isolated layer is set on the top of 7th floor of the frame and the bottom of the core tube, the isolated bearings are connected with the columns by means of consolidation. The frame isolated layer is equipped with 24 LRB500 lead-core rubber seismic isolated bearings, the core tube isolated layer is equipped with 12 LRB600 lead-core rubber seismic isolated bearings. The information of LRB500 and LRB600 lead-core rubber isolated bearings is shown in Table 3. C30 and C40 concrete non-linear materials is adopted with Takeda hysteretic type, and HRB400 reinforced non-linear materials is adopted with Kinematic

Table 1. Information of frame section

Component type	Component position (floor)	Sectional dimension (mm)	Information of reinforcing bars		
			Concrete cover thickness (mm)	Stirrup diameter (mm)	Longitudinal rib size
Frame column	1~8	600×600	50	10	16 C 22
	9~18	500×500	50	10	16 C 22
Frame beam	1~8	600×350	50	10	Bottom 4 C 20 Roof 4 C 16
	9~18	500×300	50	10	Bottom 4 C 20 Roof 4 C 16
Connecting beam	1~18	400×200	50	10	Bottom 4 C 20 Roof 4 C 16

Table 2. Information of shear wall section

Component type	Sectional name	Unit type	Concrete thickness /mm	Vertical distribution of reinforcing bars ratio
Shear wall in non-bottom strengthening zone	Wall200	Thin-shell	200	–
Shear wall with constrained edge members	Wall-Edge-200	Multi-layer shell	200	5%
Shear wall with non-constrained edge members	Wall-200	Multi-layer shell	200	0.40%

Table 3. Parameters of isolated bearings

Model	Effective diameter (mm)	Total thickness of rubber (mm)	Stiffness before yield ($kN \cdot m^{-1}$)	Equivalent stiffness		Vertical stiffness ($kN \cdot mm^{-1}$)	Yield strength (kN)	Limit displacement (mm)
				100% horizontal shear deformation ($kN \cdot m^{-1}$)	250% horizontal shear deformation ($kN \cdot m^{-1}$)			
LRB500	500	92	10910	1270	1010	2400	40.0	275
LRB600	600	110	13110	1580	1580	2800	63.0	330

hysteretic type, their stress-strain curves are shown in Figure 6. Frame columns are adopted with PMM plastic hinges, frame beams and connecting beams are adopted with M3 plastic hinges, their M-Teta curves are shown in Figure 7. The two floors at the bottom of the core tube are reinforced area, and the rest are non-reinforced area. The reinforced area is simulated by layered shells, and the non-reinforced area is simulated by elastic thin shell elements.

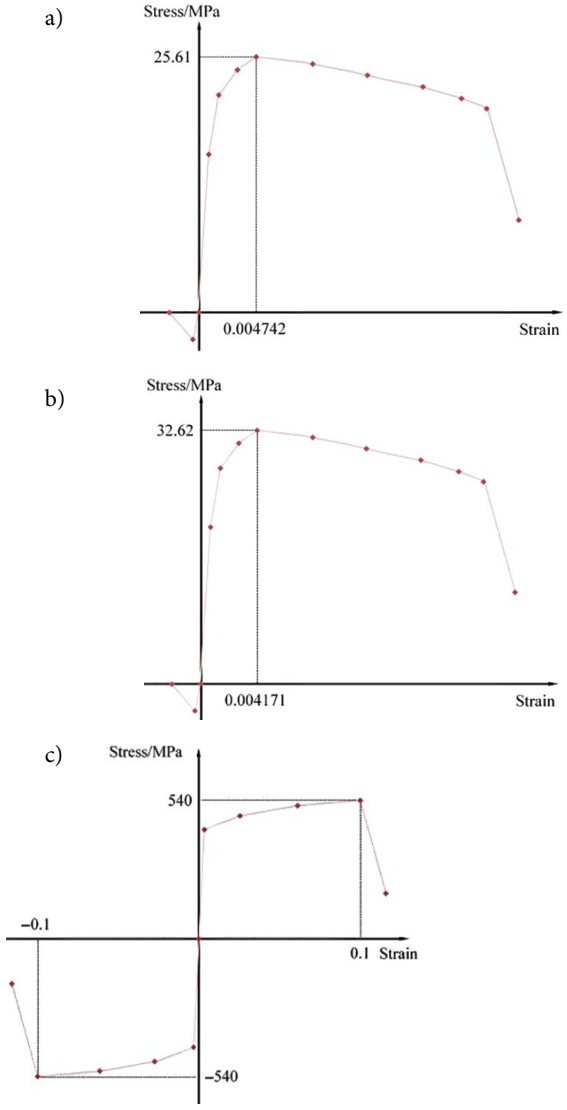

Figure 6. Stress-strain curves: a – C30; b – C40; c – HRB400

1.3. The realization of the new staggered story isolated structure considering SSI effect

Two kinds of site soils are used for comparative study. The site soil with a large shear modulus is hard soil and the site soil with a small shear modulus is soft soil. The site soils information is shown in Table 4.

Based on the site soils shear modulus, shear velocity and the thickness of shallow foundation, the point spring stiffness, damping coefficients of the interaction between the shallow foundation and the site soils are derived. By defining the relationship between the soils profile and the shallow foundation point spring parameters, the soil-structure interaction is simulated (Wang et al., 2008; National Institute of Standards and Technology [NIST], 2012). The modal period of the structure is obtained through modal analysis. The first-order modal frequency is (Computers and Structures Inc., 2007):

$$\omega = \frac{2\pi}{T}. \tag{1}$$

Substituting Eqn (1) into Eqns (2) and (3) to solve the dimensionless frequency parameters of the soils:

$$\begin{cases} \alpha_{0x} = \dfrac{\omega B}{V_{sx}} \\ \alpha_{0y} = \dfrac{\omega B}{V_{sy}}; \\ \alpha_{0z} = \dfrac{\omega B}{V_{sz}} \end{cases} \tag{2}$$

$$\begin{cases} \alpha_{0xx} = \dfrac{\omega B}{V_{sxx}} \\ \alpha_{0yy} = \dfrac{\omega B}{V_{syy}}, \\ \alpha_{0zz} = \dfrac{\omega B}{V_{szz}} \end{cases} \tag{3}$$

where B is the thickness of shallow foundation, V_{sx}, V_{sy}, V_{sz} are the lateral velocity of the soils in the x, y, z direc-

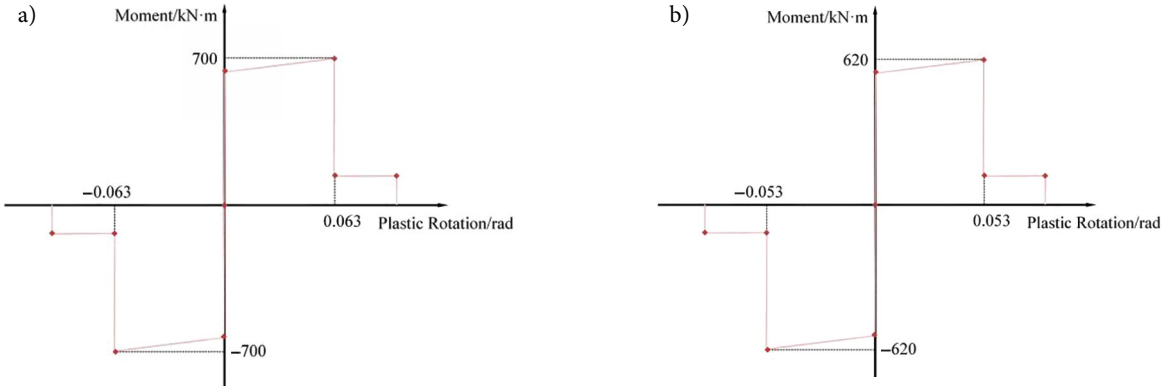

Figure 7. Plastic hinge M-Teta curves: a – PMM; b – M3

Table 4. Soils parameters

Soils type	Shear wave velocity range ($m \cdot s^{-1}$)	Shear wave velocity ($m \cdot s^{-1}$)	Density ($kg \cdot m^{-3}$)	Poisson's ratio of soil layer	Initial shear modulus of soil layer G_0 ($\times 10^4 kN \cdot m^{-2}$)	Effective shear modulus of soil layer $G = 0.42G_0$ ($\times 10^4 kN \cdot m^{-2}$)	Cohesive force (kPa)	Angle of internal friction (°)
Hard soil	$250 \le v \le 500$	400	1800	0.3	28.8	12.096	60	30
Soft soil	$150 \le v \le 500$	200	1700	0.35	6.8	2.856	25	12

tions; V_{sxx}, V_{syy}, V_{szz} are the lateral velocities of the soils on the x, y, z planes.

Substitute Eqn (2) into Eqns (4), (3) into (5) and the size of the shallow foundation to solve the damping correction coefficient of the soils:

$$\begin{cases} \alpha_x = 1.0 \\ \alpha_y = 1.0 \\ \alpha_z = 1.0 - \left[\dfrac{\left(0.4 + \dfrac{0.2}{L/B}\right)\alpha_{0z}^2}{\left(\dfrac{10}{1+3(L/B-1)}\right) + \alpha_{0z}^2} \right] \end{cases}; \tag{4}$$

$$\begin{cases} \alpha_{xx} = 1.0 - \left[\dfrac{\left(0.55 + 0.01\sqrt{L/B-1}\right)\alpha_{0xx}^2}{\left(2.4 - \dfrac{0.4}{(L/B)^3}\right) + \alpha_{0xx}^2} \right] \\ \alpha_{yy} = 1.0 - \left[\dfrac{0.55\alpha_{0yy}^2}{\left(0.6 + \dfrac{1.4}{(L/B)^3}\right) + \alpha_{0yy}^2} \right] \\ \alpha_{zz} = 1.0 - \left[\dfrac{\left(0.33 + 0.03\sqrt{L/B-1}\right)\alpha_{0zz}^2}{\left(\dfrac{0.8}{1+0.33(L/B-1)}\right) + \alpha_{0zz}^2} \right] \end{cases}, \tag{5}$$

where L is the length of the shallow foundation.

Substitute the site soils shear modulus and shear speed as well as the size of the shallow foundation into Eqns (6) and (7), obtain the spring stiffness in static state:

$$\begin{cases} k_{x,sur} = \dfrac{G_x B}{2-\nu}\left[6.8\left(\dfrac{L}{B}\right)^{0.65} + 2.4 \right] \\ k_{y,sur} = \dfrac{G_y B}{2-\nu}\left[6.8\left(\dfrac{L}{B}\right)^{0.65} + 0.8\left(\dfrac{L}{B}\right) + 1.6 \right] \\ k_{z,sur} = \dfrac{G_z B}{1-\nu}\left[3.1\left(\dfrac{L}{B}\right)^{0.75} + 1.6 \right] \end{cases}; \tag{6}$$

$$\begin{cases} k_{xx,sur} = \dfrac{G_{xx} B^3}{1-\nu}\left[3.2\left(\dfrac{L}{B}\right) + 0.8 \right] \\ k_{yy,sur} = \dfrac{G_{yy} B^3}{1-\nu}\left[3.73\left(\dfrac{L}{B}\right)^{2.4} + 0.27 \right] \\ k_{yy,sur} = G_{zz} B^3\left[4.25\left(\dfrac{L}{B}\right)^{2.45} + 4.06 \right] \end{cases}, \tag{7}$$

where G_x, G_y, G_z are the shear modulus of the soils in the x, y, z directions; G_{xx}, G_{yy}, G_{zz} are the shear modulus of the x, y, z sides of the soils; $v$is the shear velocity of the soils.

Substitute Eqns (4) and (6) into Eqn (8), and substitute Eqns (5) and (7) into Eqn (9), obtain the spring stiffness in dynamic state:

$$\begin{cases} k_x = \alpha_x \times \eta_x \times k_{x,sur} \\ k_y = \alpha_y \times \eta_y \times k_{y,sur} \\ k_z = \alpha_z \times \eta_z \times k_{z,sur} \end{cases}; \tag{8}$$

$$\begin{cases} k_{xx} = \alpha_{xx} \times \eta_{xx} \times k_{xx,sur} \\ k_{yy} = \alpha_{yy} \times \eta_{yy} \times k_{yy,sur} \end{cases}, \tag{9}$$

where η_x, η_y, η_z, η_{xx}, η_{yy}, η_{zz} is the correction coefficient.

Substitute Eqns (2), (4) and (8) into Eqn (10), and substitute Eqns (3), (5) and (9) into Eqn (11), obtain damping in six degrees of freedom directions:

$$\begin{cases} \beta_z = \left[\dfrac{4\left[\psi(L/B) + (D_e/B)(1+L/B)\right]}{(k_z/G_z B)} \right]\left[\dfrac{\alpha_{0z}}{2\alpha_z} \right] \\ \beta_y = \left[\dfrac{4\left[L/B + (D_e/B)(\psi+L/B)\right]}{(k_y/G_y B)} \right]\left[\dfrac{\alpha_{0y}}{2\alpha_y} \right] \\ \beta_x = \left[\dfrac{4\left[L/B + (D_e/B)(\psi+L/B)\right]}{(k_y/G_y B)} \right]\left[\dfrac{\alpha_{0x}}{2\alpha_x} \right] \end{cases}; \tag{10}$$

$$\begin{cases} \beta_{zz} = \left[\dfrac{\left(\frac{4}{3}\right)\left[3\frac{LD_e}{B^2}+\psi\frac{L^3D_e}{B^4}+3\frac{L^2D_e}{B^3}+\psi\frac{D_e}{B}+\frac{L^3}{B^3}+\frac{L}{B}\right]\alpha_{0zz}^2}{\left(\frac{k_{zz}}{G_{zz}B}\right)\left[\left(\frac{1.4}{1+3(L/B-1)^{0.5}}\right)+\alpha_{0zz}^2\right]}\right]\left[\frac{\alpha_{0zz}}{2\alpha_{zz}}\right] \\ \beta_{yy} = \left[\dfrac{\left(\frac{4}{3}\right)\left[\frac{L^3D_e}{B^4}+\psi\frac{LD_e^3}{B^4}+3\frac{L^2D_e}{B^3}+\psi\frac{L^3}{B^3}\right]\alpha_{0yy}^2}{\left(\frac{k_{yy}}{G_{yy}B^3}\right)\left[\left(\frac{1.8}{1+1.75(L/B-1)}\right)+\alpha_{0yy}^2\right]}+\dfrac{\left(\frac{4}{3}\right)\left(\frac{L}{B}+\psi\right)\left(\frac{D_e}{B}\right)^3}{\frac{k_{yy}}{G_{yy}B^3}}\right]\left[\frac{\alpha_{0yy}}{2\alpha_{yy}}\right] \\ \beta_{xx} = \left[\dfrac{\left(\frac{4}{3}\right)\left[\frac{D_e}{B}+\left(\frac{D_e}{B}\right)^3+\psi\frac{LD_e^3}{B^4}+3\frac{LD_e}{B^2}+\psi\frac{L}{B}\right]\alpha_{0xx}^2}{\left(\frac{k_{xx}}{G_{xx}B^3}\right)\left[\left(\frac{1.8}{1+1.75(L/B-1)}\right)+\alpha_{0xx}^2\right]}+\dfrac{\left(\frac{4}{3}\right)\left(\psi\frac{L}{B}+1\right)\left(\frac{D_e}{B}\right)^3}{\frac{k_{xx}}{G_{xx}B^3}}\right]\left[\frac{\alpha_{0xx}}{2\alpha_{xx}}\right] \end{cases} \quad (11)$$

The radiation damping ratio in the formula is $\psi=\sqrt{2(1-\nu)/(1-2\nu)}$; $\psi \le 2.5$; D_e is the pile spacing.

Substitute Eqns (1), (8) and (10) into Eqn (12), and substitute Eqns (1), (9) and (11) into Eqn (13), obtain damping coefficient in six degrees of freedom directions:

$$\begin{cases} c_x = \dfrac{2(\beta_s+\beta_x)k_x}{\omega} \\ c_y = \dfrac{2(\beta_s+\beta_y)k_y}{\omega} \\ c_z = \dfrac{2(\beta_s+\beta_z)k_z}{\omega} \end{cases}; \quad (12)$$

$$\begin{cases} c_{xx} = \dfrac{2(\beta_s+\beta_{xx})k_{xx}}{\omega} \\ c_{yy} = \dfrac{2(\beta_s+\beta_{yy})k_{yy}}{\omega} \\ c_{zz} = \dfrac{2(\beta_s+\beta_{zz})k_{zz}}{\omega} \end{cases}. \quad (13)$$

In summary, the SSI effect is realized by simulating the point spring stiffness, damping and damping coefficient of the interaction between the shallow foundation and the site soils.

1.4. Information of seismic waves

According to the provisions of China's code for seismic design of building, the site is classified as class II or III, the ground motion is selected by building site classification and design seismic group (Ministry of Housing and Urban-rural Construction of the People's Republic of China and the General Administration of Quality Supervision, Inspection and Quarantine of the People's Republic of China, 2016). Therefore, Nanjing wave which is suitable for the class II site soil, Tianjin wave and Lanzhou wave which are suitable for the class III site soil are selected, which meet the design requirements of the code. Three ground motions records in Nanjing, Tianjin and Lanzhou are selected form the Pacific Earthquake Center of the United States. The basic information of ground motion is shown in Table 5, and the acceleration response spectrum of ground motion is shown in Figure 8.

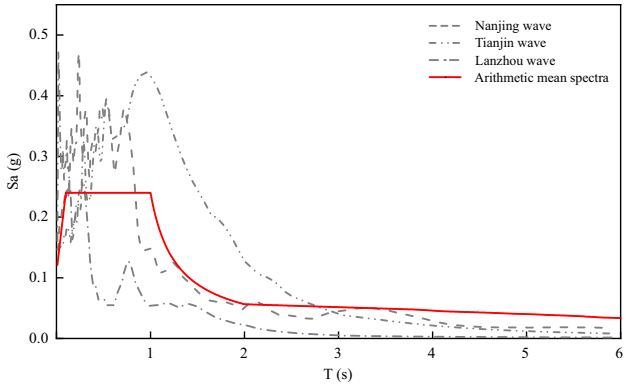

Figure 8. Acceleration spectra of selected ground motion records

Table 5. Information of ground motion

Ground motion	Magnitude	Epicentral distance (km)	PGA ($cm \cdot s^{-2}$)
Nanjin wave	6.9	25	42.8
Tianjin wave	6.9	65	145.8
Lanzhou wave	6.8	32	196.2

2. Study on seismic response of the new staggered story isolated structure considering SSI

2.1. Modal analysis

The modal periods of the new staggered story isolated structure are shown in Table 6.

Table 6. Modal periods of new staggered story isolated structures

Modal period	Regardless of the SSI effect	Considering SSI effect (hard soil)	Considering SSI effect (soft soil)
T1/s	3.196	5.164	5.675
T2/s	2.972	3.857	4.111
T3/s	2.798	3.294	3.331
T4/s	1.001	1.11	1.111
T5/s	0.956	1.066	1.068
T6/s	0.918	1.019	1.02

It can be seen from Table 6 that compared with the new staggered story isolated structure without considering SSI effect, the new staggered story isolated structure considering SSI effect has weaker stiffness, which causes the modal period to be extended, the softer the soil, the more obvious it is.

2.2. The seismic response of the new staggered story isolated structure considering SSI effect

Above the 8th floor (isolated layer of the frame), the core tube is integrated with the frame, so their inter-layer acceleration and inter-layer drift angle are the same, below the 8th floor, the core tube is separated from the frame, so their inter-layer acceleration and inter-layer drift angle

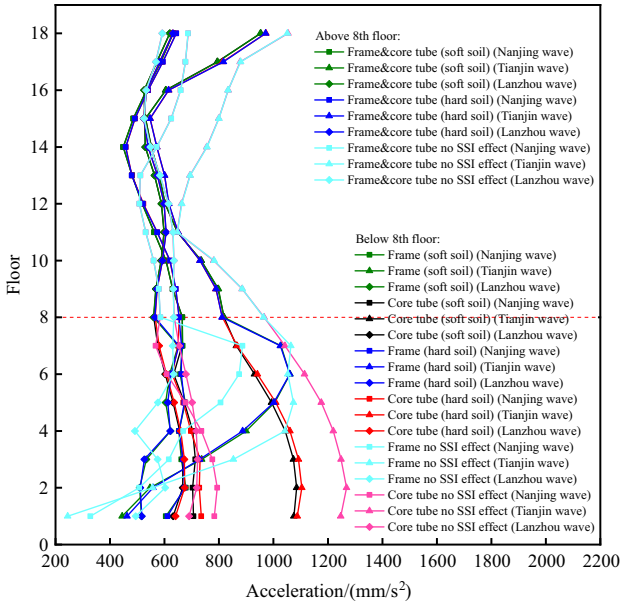

Figure 9. Comparison of inter-layer acceleration

are inconsistent. The comparison of inter-layer acceleration between the new staggered story isolated structure considering SSI effect and without considering SSI effect is shown in Figure 9.

It can be seen from Figure 9 that the acceleration response of the new staggered story isolated structure decreases when SSI effect is considered. The accelerations of the new staggered story isolated structure decrease in soft site soil than that in hard site soil.

The comparison of inter-layer drift angle is shown in Figure 10.

It can be seen from Figure 10 that the inter-layer drift angle of the structure is within 0.0014, and the inter-layer drift angle of the seismic isolated layer is within 0.0038, which does not exceed the China design code requirements (GB 50011-2010) (Ministry of Housing and Urban-rural Construction of the People's Republic of China and the General Administration of Quality Supervision, Inspection and Quarantine of the People's Republic of China, 2016).

It can be seen from Figures 10a and 10b that the frame and the core tube are integrated above the 8th floor (the position of the frame isolated layer), the inter-layer drift angle considering the SSI effect is less than regardless of the SSI effect. The frame below the8th floor is separated from the core tube, the inter-layer drift angle of the core tube considering the SSI effect is close to that regardless of the SSI effect, and the inter-layer drift angle of the frame considering the SSI effect reduced than regardless of the SSI effect.

It can be seen from Figure 10c that the inter-layer drift angle above 8th floor (the position of the frame isolated layer) in soft site soil are close to that in hard site soil. The core tube and the frame inter-layer drift angle below the 8th floor in soft site soil is smaller than that of the hard site soil.

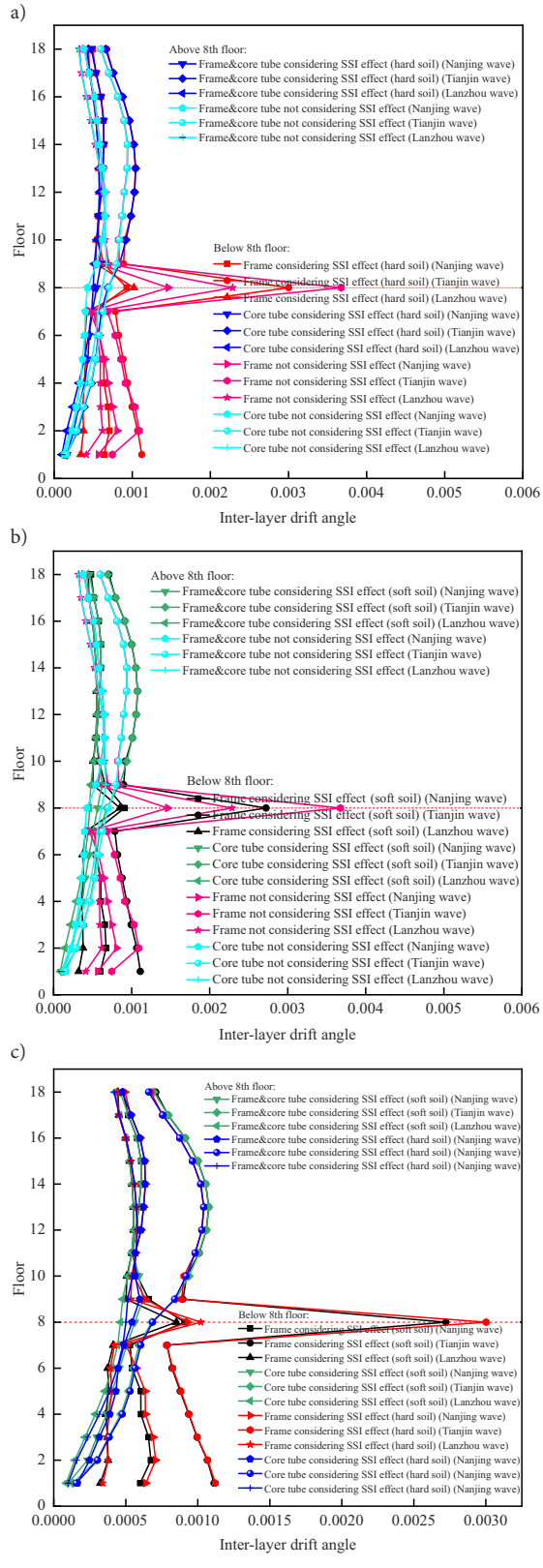

Figure 10. Comparison of inter-layer drift angle: a – comparison of inter-layer drift angle between the new staggered story isolated structure considering SSI effect and not considering SSI effect (hard soil); b – comparison of inter-layer drift angle between the new staggered story isolated structure considering the SSI effect and not considering the SSI effect (soft soil); c – comparison of inter-layer drift angle between different sites soils considering the SSI effect

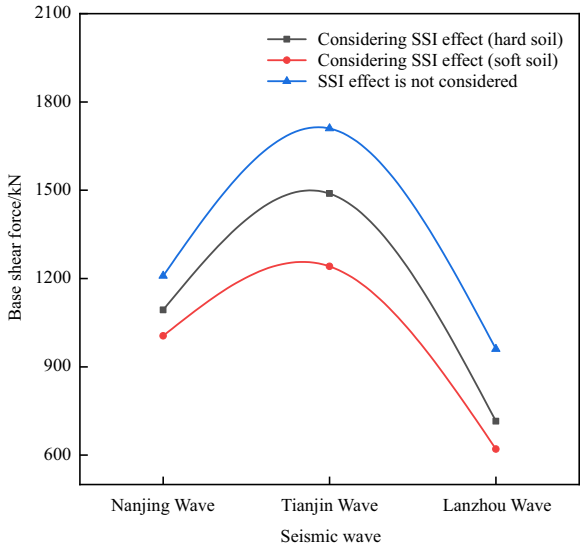

Figure 11. Comparison of base shear force

The comparison of the base shear force is shown in Figure 11.

It can be seen from Figure 11 that the base shear force considering SSI effect is less than regardless of SSI effect. The base shear force considering the SSI effect in soft site soil is less than that in the hard site soil.

The shear force comparison of the frame is shown in Figure 12.

The blue circle in Figure 12 is the maximum point of frame shear force. The shear force value in Figure12a is between 50~60 kN, in Figure 12b is between 70~90 kN, in Figure 12c is between 90~110 kN.

It can be seen from Figure 12 that the shear force of the frame considering the SSI effect is greater than that without the SSI effect, the softer the site soil, the more the frame shear force increases.

The shear force comparison of the core tube is shown in Figure 13. The color from blue to purple indicates that the shear force from large to small.

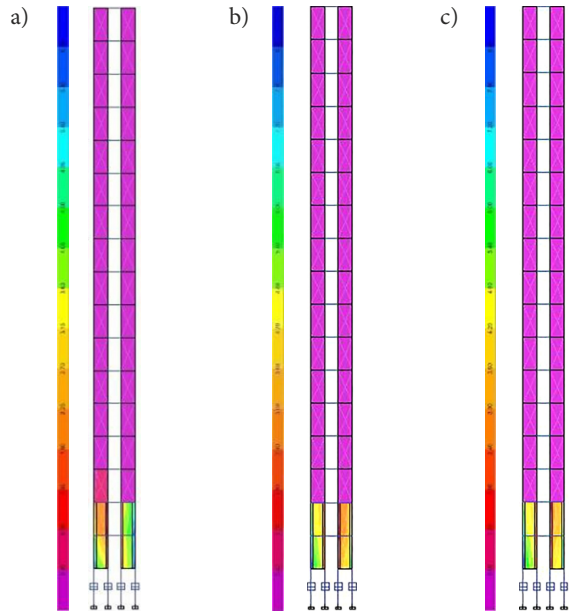

Figure 13. Comparison of shear forces of the core tube: a – shear force of the core tube without considering the SSI effect; b – shear force of the core tube considering SSI effect (hard soil); c – shear force of the core tube considering SSI effect (soft soil)

It can be seen from Figure 13 that the shear force of the core tube that considers the SSI effect is less than that regardless of the SSI effect, the softer the site soil, the more obvious those changes are. The shear force transfers from the core tube to the frame. Considering the SSI effect or not, the larger shear force position is similar, both are located on the two floors above the isolated layer.

3. The damage of the new staggered story isolated structure considering the SSI effect

Through comparative analysis, the damage of the new staggered story isolated structure is different between considering SSI effect and regardless of the SSI effect.

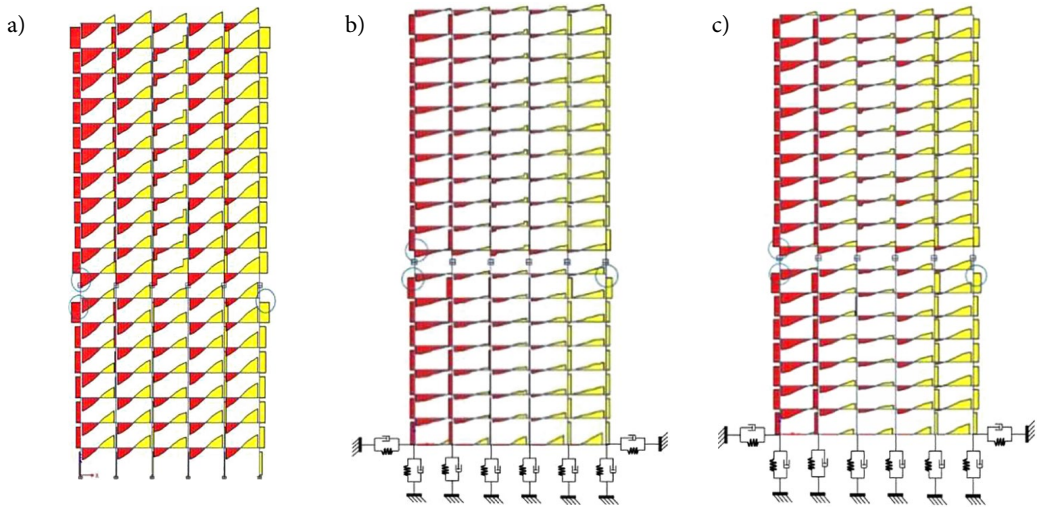

Figure 12. Shear force comparison of frame: a – shear force of frame without considering the SSI effect; b – shear force of frame considering SSI effect (hard soil); c – shear force of frame considering SSI effect (soft soil)

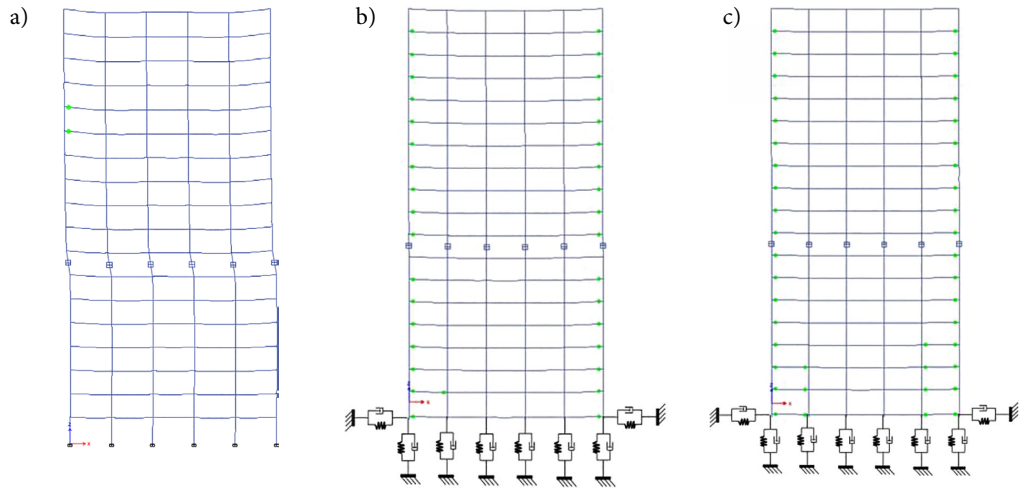

Figure 14. Comparison of plastic hinges situation (Green dots are plastic hinges): a – the plastic hinge situation of frame without considering the SSI effect; b – the plastic hinge situation of frame considering SSI effect (hard soil); c – the plastic hinged situation of frame considering SSI effect (soft soil)

Figure 14 shows the comparison of the plastic hinges of the frame.

It can be seen from Figure 14 that the plastic hinge considering the SSI effect increases, and the damage increases. The softer the site soil, the more plastic hinges and the greater the damage is.

The stress comparison of the core tube is shown in Figure 15. The color from blue to purple indicates that the stress from large to small.

It can be seen from Figure 15 that the stress damage of the core tube considering the SSI effect reduced, the softer the site soil, the smaller the core tube damage is. The serious damage position of the core tube between considering the SSI effect and not considering the SSI effect is similar, both are the three floors above the core tube seismic isolated layer.

Under each seismic wave, the hysteresis curve of the seismic isolated bearings at the frame and the core tube is shown in Figure 16. The corner seismic isolated bearings are selected because the seismic isolated bearings at these positions deforms greatly.

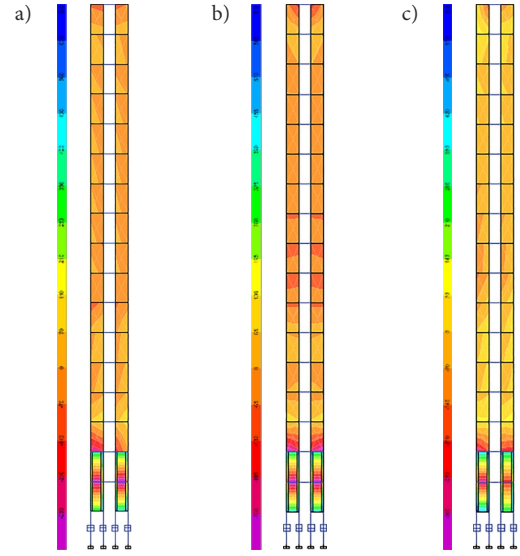

Figure 15. Stress damage comparison of core tube: a – stress damage of the core tube without considering the SSI effect; b – stress damage of the core tube of considering SSI effect (hard soil); c – stress damage of the core tube of considering SSI effect (soft soil)

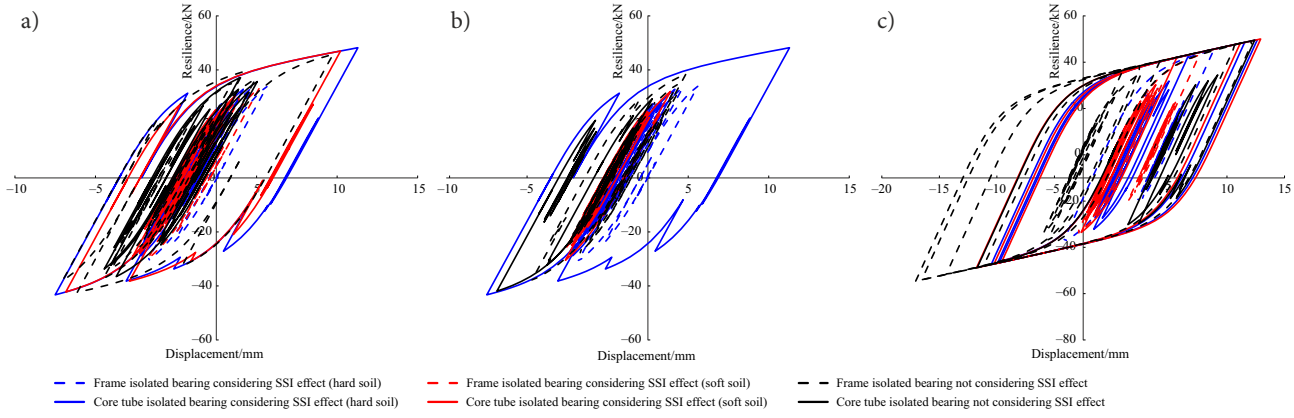

Figure 16. Hysteretic curve of isolated bearings: a – hysteresis curve of seismic isolated bearing under Nanjing wave; b – hysteresis curve of seismic isolated bearing under Lanzhou wave; c – hysteresis curve of seismic isolated bearing under Tianjin wave

It can be seen from Figure 16 that the energy absorption of the seismic isolated bearings of the frame reduces when considering the SSI effect. The hysteresis curve of the seismic isolated bearings of the core tube is full and the energy absorption increase when considering the SSI effect the softer the site soil, the more obvious the trend is.

Conclusions

A new staggered story isolated structure model considering the SSI effect is established. The SSI effect is simulated by using the soils profile and the point springs of the shallow foundation. The dynamic time history analysis under rare earthquakes is performed, while soils is divided into hard soil and soft soil for comparative analysis. The conclusions are listed as follows:

(1) By considering the SSI effect, the stiffness of the new staggered story isolated structure reduced, the modal period extended and the seismic response reduced the softer the site soil, the more obvious those changes are.
(2) By considering the SSI effect, the base shear force of the structure decreases, the softer the site soil, the more obvious those changes are.
(3) By considering the SSI effect, the new staggered story isolated structure shear force and the damage of the core tube decreases, while the shear force and the damage of the frame increases, the shear force transfers from the core tube to the frame.
(4) By considering the SSI effect, the energy absorption of the isolated bearings of the frame reduces. The hysteresis curve of the isolated bearings of the core tube is full and the energy absorption increase. The softer the site soil, the more obvious the trend is.

Acknowledgements

The authors gratefully acknowledge the financial support of National Natural Science Foundation of China (No. 52168072 & No. 51808467), High-level Talents Support Plan for "Ten Thousand Talents" of Yunnan Province (2020) and PhD Start-up Fund of Southwest Forestry University.

Conflict of interests

The authors declare that there is no conflict of interests regarding the publication of this paper.

Data availability statement

All data included in this study are available upon request by contact with the corresponding author.

References

Castaldo, P., & Tubaldi, E. (2018). Influence of ground motion characteristics on the optimal single concave sliding bearing properties for base-isolated structures. *Soil Dynamics & Earthquake Engineering*, *104*, 346–364. https://doi.org/10.1016/j.soildyn.2017.09.025

Chang, P. J., & Zhu, J. (2011). Seismic vulnerability analysis of mid-story isolation and reduction structures based stochastic vibration. *Advanced Materials Research*, *243–249*, 3988–3991. https://doi.org/10.4028/www.scientific.net/AMR.243-249.3988

Computers and Structures Inc. (2007). *Analysis reference manual for SAP2000*, *ETABS*, *and SAFE*.

Karabork, T., Deneme, I. O., & Bilgehan, R. P. (2014). A comparison of the effect of SSI on base isolation systems and fixed-base structures for soft soil. *Geomechanics and Engineering*, *7*(1), 87–103. https://doi.org/10.12989/gae.2014.7.1.087

Kelly, J. M. (2012). Base isolation: Linear theory and design. *Earthquake Spectra*, *6*(2), 223–244. https://doi.org/10.1193/1.1585566

Kubin, J., Kubin, D., Özmen, A., Şadan, O. B., & Eroglu, E. (2012). Seismic retrofit of an existing multi-block hospital by seismic isolators. In *Proceedings of the 15th World Conference on Earthquake Engineering*, Lisbon, Portugal.

Li, H., Wang, Y. N., & Du, Y. F. (2012). Influence of soil structure dynamic interaction on base isolated structure. *Earthquake Resistant Engineering and Retrofitting*, *34*(1), 37–41.

Liu, W. Q., Li, C. P., Wang, S. G., Du, D. S., & Wang, H. (2013). Comparative study on high-rise isolated structure founded on various soil foundation by using shaking table tests. *Journal of Vibration and Shock*, *32*(16), 128–133.

Liufu, J., Lin, S. M., & Huang, Z. H. (2020). Structural scheme selection and design of an isolated high-rise building structure with a large chassis and multiple tower-layer in a high-intensity region. *Building Structure*, *50*(10), 83–89.

Loh, C. H., Weng, J. H., Chen, C. H., & Lu, K. C. (2013). System identification of mid-story isolation building using both ambient and earthquake response data. *Structural Control and Health Monitoring*, *20*(2), 139–155. https://doi.org/10.1002/stc.479

Ministry of Housing and Urban-rural Construction of the People's Republic of China and the General Administration of Quality Supervision, Inspection and Quarantine of the People's Republic of China. (2016). *Code for seismic design of buildings* (No. GB 50011-2010). China Architecture & Building Press.

National Institute of Standards and Technology. (2012). *Soil-structure interaction for building structures* (Report No. NIST/GCR 11-917).

Qi, Y. N., Sun, R., Guan, Q. S., & Zeng, C. W. (2020). Application of new type anti-tension device in high aspect ratio isolation structure design. *Earthquake Resistant Engineering and Retrofitting*, *42*(4), 93–98.

Shan, J., Shi, Z., Gong, N., & Shi, W. (2020). Performance improvement of base isolation systems by incorporating eddy current damping and magnetic spring under earthquakes. *Structural Control and Health Monitoring*, *27*(6), e2524. https://doi.org/10.1002/stc.2524

Shang, S. P., & Hu, L. H. (2020). Analysis of energy dissipation characteristics of base isolation structures. *Earthquake Engineering and Engineering Dynamics*, *40*(1), 12–21.

Su, Y., Li, J. Z., He, Q., Bao, X., & Li, A. Q. (2015). Related parameter analysis of story isolation structure considering soil-structure interaction. *Industrial Construction*, *45*(11), 9–13.

Wang, Y. R., Dai, J. W., Zhan, S. M., & Jiang, Y. (2008). A numerical analysis based substitute method for shaking table test in considering of the soil-structure interaction. In *The 14th World Conference on Earthquake Engineering*, Beijing, China.

Zhang, Y. Q. (2019, December 2). Seismic artifact for high-rise buildings in our city. *Baotou Daily*, *7*.

Zhang, Y., Yi, W. J., Tan, P., & Zhou, F.-L. (2009). The dynamic reliability of mid-story isolation structure under seldomly occurred earthquake. *Journal of Hunan University* (*Natural Sciences*), *36*(3), 11–15.

Zhang, S. R., Tan, P., Du, Y. F., Bao, C., & Zhou, F. L. (2014). Effect analysis of soil-structure interaction on inter-story isolation structure. *China Civil Engineering Journal*, *47*(S1), 246–252.

Zhou, Q., Singh, M. P., & Huang, X. (2016). Model reduction and optimal parameters of mid-story isolation systems. *Engineering Structures*, *124*, 36–48. https://doi.org/10.1016/j.engstruct.2016.06.011

Zhou, Y., Li, X., & Chen, Z. (2018). Seismic responses analysis of base-isolated LNG storage tank. In *Proceedings of GeoShanghai 2018 International Conference: Advances in Soil Dynamics and Foundation Engineering*, Shanghai, China. https://doi.org/10.1007/978-981-13-0131-5_36

Zhuang, H. Y., Yu, X., Zhu, C., & Jin, D. (2014). Shaking table tests for the seismic response of a base-isolated structure with the SSI effect. *Soil Dynamics and Earthquake Engineering*, *67*, 208–218. https://doi.org/10.1016/j.soildyn.2014.09.013